Orbital Constraints on Exoplanet Habitability

Zachery McBrearty

Level 4 Project, MPhys Physics with Astronomy

Supervisor: Dr Richard Wilman

Second Supervisor: Dr Craig Testrow

Department of Physics, Durham University

Submitted: January 18, 2024

A 1-D energy balance climate model is developed in order to investigate how changing certain orbital parameters can result in changes to a planet's habitability. Theoretical relationships between temperature, semimajoraxis, and eccentricity are derived from a simple 0-D energy balance model and are tested against the 1-D model and are found to be correct. A qualitative analysis of obliquity shows that there are optimal obliquities to minimise and maximise global temperature. The climates of exomoons orbiting gas giants are also investigated, including reflected light from the gas giant, eclipsing, and tidal heating. It is expected that these additional sources of heat move the habitable zones for the planet outwards.

CONTENTS

1. INTRODUCTION

The climate of a planet such as the Earth is many dimensional and thus very complicated. However, understanding and predicting the climate of a planet is essential for predicting the effects of climate change and finding habitable exo-planets. Fully simulating the entire atmosphere, ocean, and land would be extremely difficult without the use of massive supercomputers. By reducing degrees of freedom in the model, the simulation can become feasible while still yielding useful and valid results.

The simplest climate model is a 0 dimensional energy balance. The 0-D model is an equality of the input energy from the Sun (LHS) to the output energy from the Earth acting as a black body (RHS),

$$\pi r^2 S(1 - A) = 4\pi r^2 \sigma T^4, \tag{1}$$

where r is the radius of the planet, T is the global average temperature of the planet, S is the incident solar radiation (insolation), A is the reflectance (albedo), and σ is the Stefan-Boltzmann constant. This 0-D model does not resolve the surface or any features of the planet, and treats the planet as homogeneous. This means that the model is quick to compute and provides a good baseline for further computation. By plugging in values for the Earth, a global temperature of $-18°C$ is found; well below the global average value of $14°C$ from 1951 to 1980 [10]. One reason for this is a lack of greenhouse effect, meaning the planet emits much more radiation than it should. Another problem with the model is that it is not dynamic, meaning seasonal changes due to eccentricity or obliquity are not included.

A 1-D Energy Balance Climate Model (here on EBCM) resolves the surface of the planet into latitude bands which have an (longitude-averaged) ocean-land fraction with variable heat capacity and albedo. Each of these latitude bands is treated as balancing incoming solar flux (insolation) with energy out via blackbody radiation. There is also an additional energy diffusion term for energy transport between latitude bands. The form of the EBCM from Williams and Kasting 1997 (here on WK97) is given as

$$C\frac{\partial T(x,t)}{\partial t} - D\frac{\partial}{\partial x}\left((1-x^2)\frac{\partial T(x,t)}{\partial x}\right) + I - S(1-A) = 0 \tag{2}$$

where $x = \sin\lambda$, λ is the latitude, C is the heat capacity of the latitude band, D is the diffusion coefficient determining how effective the diffusion is, I is the IR-emission of the band, S is the insolation, and A is the planetary albedo. All these parameters can be dependent on time and space, but generally in the program only a few are. These parameters, as well has the numerical integration of the EBCM, are explored in Section 2.

This EBCM can be extended very easily for other heat sources. In Section 3 the parameterisation and habitability of an exomoon around a gas giant is explored. This requires additional parameters for the energy input due to emission from the gas giant and tidal heating due to the moon's orbit.

It is expected that moons around gas giants which are close to the parent star (hot jupiters, hot neptunes etc.) could have warm and potentially habitable exomoons. This is bolstered by the potential for an exomoon to be tidally heated, thus not dependent on the central star for life to exist. This is seen in our own solar system in the investigations of Io and Enceladus [11].

Tidal heating is also important for the discovery of exomoons. The high temperatures of these tidally heated moons can create peak emission temperatures different from the star and gas giant allowing for easier detection. Furthermore, the volcanic activity of these moons can also eject plumes of material giving indication of the presence and physical makeup of the moon [12].

In Section 4 the parameters making up the EBCM are varied to see effects on the temperature profile and habitability ranges. This work could inform about the habitability of exoplanets and the seasonal variations they may undergo. Additionally, the work with an extra heat source such as tidal heating informs how an exoplanet's climate and habitable zones may change due to other forcing.

Section 5 deals with developing and working with an Energy Balance Depth Model (EBDM) to investigate if a planet could sustain life under a frozen surface due to tidal heating.

2.   1D ENERGY BALANCE CLIMATE MODEL

A.   Transforming from x to λ

While the EBCM is originally specified in sine of latitude it is better to work and integrate in terms of latitude, this necessitates a change of variables.

The partial derivative operator is given by

$$\frac{\partial}{\partial x} = \frac{\partial \lambda}{\partial x}\frac{\partial}{\partial \lambda} = \frac{1}{\sqrt{1-x^2}}\frac{\partial}{\partial \lambda} = \frac{1}{\cos \lambda}\frac{\partial}{\partial \lambda}, \tag{3}$$

thus the second order operator is

$$\frac{\partial^2}{\partial x^2} = \frac{1}{\cos \lambda}\frac{\partial}{\partial \lambda}\left(\frac{1}{\cos \lambda}\frac{\partial}{\partial \lambda}\right)$$
$$= \frac{\tan \lambda}{\cos^2 \lambda}\frac{\partial}{\partial \lambda} + \frac{1}{\cos^2 \lambda}\frac{\partial^2}{\partial \lambda^2}, \tag{4}$$

Fully expanding the derivatives in the EBCM assuming D is not a function of space,

$$C\frac{\partial T}{\partial t} = S(1-A) - I - 2xD\frac{\partial T}{\partial x} + D(1-x^2)\frac{\partial^2 T}{\partial x^2}, \tag{5}$$

and then subbing in eqns. (3) and (4),

$$C\frac{\partial T}{\partial t} = S(1-A) - I - D\tan \lambda\frac{\partial T}{\partial \lambda} + D\frac{\partial^2 T}{\partial \lambda^2} \tag{6}$$

which obviously diverges to infinity at the North and South poles as $\tan(\lambda \to \pm\pi/2) \to \infty$ unless $D(\lambda = \pm\pi/2) = 0$ or $\partial T/\partial \lambda|_{\lambda=\pm\pi/2} = 0$. Following Spiegel et al 2008 (here on SMS08), we choose the latter [4].

B.   Characterising model parameters

In this analysis we adopt the form of the heat capacity given by WK97. In short: $C(\lambda, t)$ varies with latitude through the ocean-land fraction, $f_o(\lambda)$, and with Temperature through the

ice-ocean fraction, $f_i(T)$, as

$$C(\lambda, T) = (1 - f_o(\lambda))C_{land} + f_o(\lambda)((1 - f_i(T))C_{ocean} + f_i(T)C_{ice}(T)),$$

Where $C_{land} = 5.25 \times 10^6$ Jm^{-2}K^{-1} and $C_{ocean} = 40 \times C_{land}$ are constant, and

$$C_{ice}(T) = \begin{cases} 9.2C_{land} & T \geq 263K \\ 2.0C_{land} & T < 263K, \end{cases}$$

We also use the diffusion coefficient from WK97 which is constant in space and time, but varies with orbital and atmospheric parameters as,

$$\frac{D}{D_0} = \frac{p}{p_0} \frac{c_p}{c_{p,0}} \left(\frac{m}{28}\right)^{-2} \left(\frac{\Omega}{1\text{day}^{-1}}\right)^{-2}$$

where $D_0 = 0.56$ Wm^{-2}K^{-1} is from fitting to the time averaged Earth model from North and Coakley 1979 [7]. p is the atmospheric pressure relative to $p_0 = 101$ kPa. c_p is the heat capacity of the atmosphere, relative to $c_{p,0} = 1 \times 10^3$ g^{-1}K^{-1}. m is the (average) mass of the particles in the atmosphere, relative to the Nitrogen molecule. Ω is the rotation rate of the planet, relative to Earth's 1 rotation per day. This can be extended to be time variable, such as having CO_2 emissions increase pressure, change heat capacity, and increase mass of particles. However varying the rotation rate of the planet is considered.

IR-emission and Albedo functions are taken from WK97. Following the example of SMS08 and Dressing et al 2010 (here on Dressing10) [1] the second set of IR and Albedo functions which are given by

$$I(T) = I_2(T) = \frac{\sigma T^4}{1 + 0.5925(T/273K)^3}$$

$$A(T) = A_2(T) = 0.525 - 0.245 \tanh\left(\frac{T - 268K}{5}\right),$$

are used in all models. This IR-emission is a blackbody radiation term (numerator) damped the optical thickness of the atmosphere (denominator) which is roughly equivalent to a greenhouse gas effect. The albedo function is a smooth scaling from low to high reflectivity due to snow and water-vapour reflectance.

The insolation function, S, is defined in WK97 as the day averaged incident (based on latitude) radiation from the sun,

$$S(\lambda, t) = \frac{q_0}{\pi} \left(\frac{1\text{ au}}{a}\right)^2 (H(t)\sin\lambda\sin\delta(t) + \cos\lambda\cos\delta(t)\sin H(t))$$

where $q_0 = 1360$ Wm^{-2} is the insolation from the Sun, a is the distance from the Sun in radians, $\cos(H(t)) = -\tan\lambda\tan\delta(t)$ is the radian half-day length with $0 < H < \pi$, and $\delta(t)$ is the solar declination defined by

$$\sin(\delta(t)) = -\sin(\delta_0)\cos(L_s(t) + \pi/2)$$

where δ_0 is the obliquity of the planet and $L_s(t) = \omega t$ is orbital longitude from an orbital angular velocity found by Kepler's laws.

C. Discretisation of the PDE

To numerically integrate the EBCM must be transformed into a discrete form. Spatially the planet can be split into a number of nodes, S, each separated by

$$\Delta\lambda = \frac{\pi^{\text{rad}}}{S-1} = \frac{180°}{S-1},$$

with spatial indexing of each zone from $m = 0, 1, \ldots, S-1$. A temporal indexing of $n = 0, 1, \ldots$ is used to discretise time into steps of Δt.

The spatial derivatives can then be approximated by the numerically stable central difference and second order central difference:

$$\frac{dT_n^m}{d\lambda} = \frac{T_n^{m+1} - T_n^{m-1}}{2\Delta\lambda}, \tag{7}$$

$$\frac{d^2T_n^m}{d\lambda^2} = \frac{T_n^{m+2} - 2T_n^m + T_n^{m-2}}{(2\Delta\lambda)^2}, \tag{8}$$

and the temporal derivative can be approximated as a forward difference,

$$\frac{dT_n^m}{dt} = \frac{T_{n+1}^m - T_n^m}{\Delta t}, \tag{9}$$

with numerical instability analysed in Section 2 D. The PDE can then be numerically integrated by solving for T_{n+1}^m using the parameters at timestep n.

However, a problem arises at the poles and edges (one in from the poles) as $m = -1, m = -2, m = S$, and $m = S+1$ are not defined. To combat this the poles ($m = 0, m = S-1$) and edges ($m = 1, m = S-2$) must be handled with more care.

Following the example of SMS08, the first spatial derivative is set to zero at the poles. Then the south $[m = 0]$ (north $[m = S-1]$) pole can be approximated by forward then backward (backward then forward) differences as follows,

$$\frac{d^2T_n^{m=0}}{d\lambda^2} = \left(\frac{dT_n^{m=1}}{d\lambda} - \frac{dT_n^{m=0}}{d\lambda}\right)/\Delta\lambda \qquad = \frac{T_n^{m=1} - T_n^{m=0}}{(\Delta\lambda)^2} \tag{10}$$

$$\frac{d^2T_n^{m=S-1}}{d\lambda^2} = \left(\frac{dT_n^{m=S-1}}{d\lambda} - \frac{dT_n^{m=S-2}}{d\lambda}\right)/\Delta\lambda = \frac{T_n^{m=S-2} - T_n^{m=S-1}}{(\Delta\lambda)^2} \tag{11}$$

where $dT_n^{m=0}/d\lambda = dT_n^{m=S-1}/d\lambda = 0$. This treatment addresses the missing indices while still maintaining a suitable level of stability (see 2 D). Similarly, the south edge ($i = 1$) uses a central-backward difference, and the north edge ($i = S-2$) uses a central-forward difference.

D. Numerical stability of time forward-difference

The general stability of the model can be understood by following the recipe for Von Neumann Stability Analysis provided in 'Numerical Modelling in a nutshell' [9]. The model is however quite complex and does not easily yield to the methods provided. Therefore the model is approximated to be in an equilibrium such that the energy input and output which are not from diffusion are equal. When unstable the model will not reach this equilibrium, meaning the following is a lowerbound for instability.
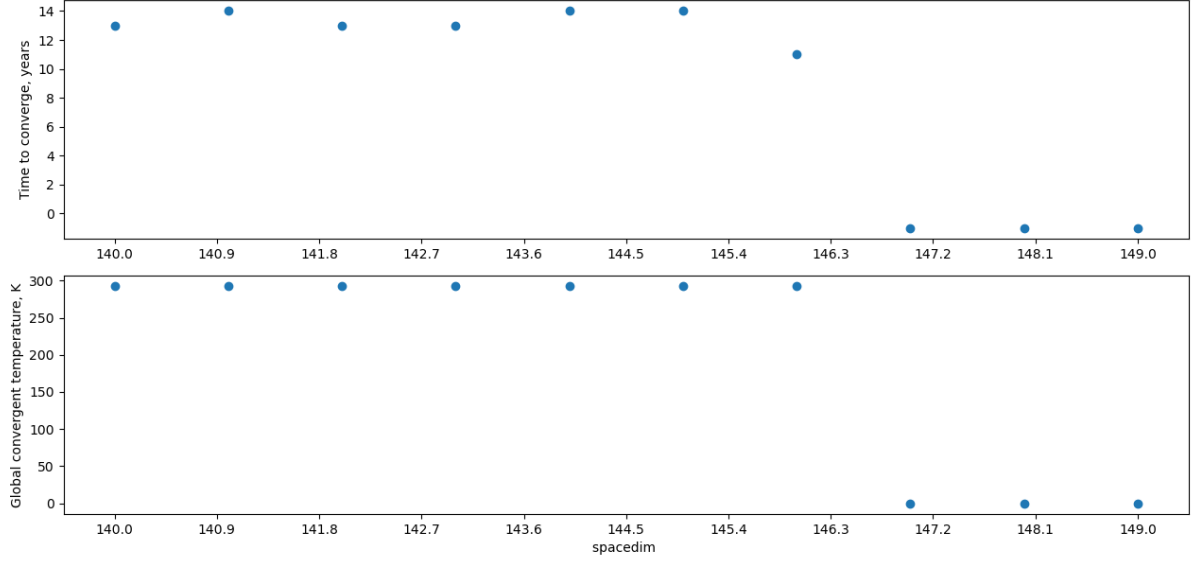
FIG. 1: The convergence (Section 4) of a series of Earth-like models with varying spatial dimension (x-axis). Top: The time in years for the system to converge to a steady temperature, Bottom: the temperature converged to. The values of time and temperature of -1 are when the model breaks and diverges to infinity. The temperatures and times taken to converge are roughly constant until the numerical instability. This instability occurs around $1.23°$ separation (146 spatial nodes) in rough agreement with the calculated value of $1.03°$.

First, assume that the equilibrum PDE can be solved with a planewave solution of the form

$$T_n^m = \xi^n \exp\left(ikm\Delta\lambda\right) \tag{12}$$

where ξ is a (complex) scaling factor which determines the growth characteristics of the plane wave, and k is the spatial frequency of the planewave. There are three cases for the value of ξ:

$$|\xi|^2 \begin{cases} > 1 & \text{growing mode, unstable} \\ = 1 & \text{completely stable} \\ < 1 & \text{decaying mode, stable} \end{cases} \tag{13}$$

In appendix A the EBCM is set to an equilibrium, discretised, and then eqn. (12) is plugged in and ξ is solved for. This process leads to the stability condition for the standard system given by (A1). It is repeated here for clarity:

$$g\Delta t \left(\tan^2(\lambda_m) + \frac{\sin^2(k\Delta\lambda)}{\Delta\lambda^2}\right) \begin{cases} > 2 & \text{growing mode, unstable} \\ = 2 & \text{completely stable} \\ < 2 & \text{decaying mode, stable} \end{cases} \tag{14}$$

where $g = D/C$ with diffusion D and heat capacity C, and k is the wavenumber of a planewave solution.

At the equator $\lambda_m = 0$, thus $\tan(\lambda_m) = 0$. This gives a stability condition of

$$g\Delta t \left(\frac{\sin^2(k\Delta\lambda)}{\Delta\lambda^2}\right) \leq 2 \tag{15}$$

and, since $|\sin(x)| \leq 1$, the model is always stable at the equator for

$$\Delta\lambda \geq \sqrt{\frac{g\Delta t}{2}}$$

It should be noted that due to the $\tan(\lambda_m)$ term the required $\Delta\lambda$ increases moving from the equator to poles. Stability at the poles is never achieved in eqn. (14), but can be recovered by the imposition that the first spatial derivative is 0 at the poles. This gives a polar stability condition given by eqn. (A2) and is also repeated here:

$$\frac{g\Delta t}{\Delta\lambda^2} \begin{cases} > 1 & \text{growing mode, unstable} \\ = 1 & \text{completely stable} \\ < 1 & \text{decaying mode, stable} \end{cases} \tag{16}$$

where again $g = D/C$ with diffusion D and heat capacity C, and k is the wavenumber of a planewave solution. Some simple manipulation gives that the poles are always stable for

$$\Delta\lambda \geq \sqrt{g\Delta t}, \tag{17}$$

which is a stricter criteria than for the equator by a factor of $\sqrt{2}$. This stricter criteria, moving from equator to pole, is why the model tends to go break and go to infinity at the poles first.

Equations (14) and (16) may be used to find the lowerbound for when the system will be unstable. Standard values for the system include a timestep of $\Delta t = 1$ day and $D = 0.56 \text{ Wm}^{-2}\text{K}^{-1}$. The heat capacity will however be variable, depending on land-ocean fraction and ocean-ice fraction.

The heat capacity is at it's lowest for the land-only system at $C = 5.25 \times 10^6 \text{ Jm}^{-2}\text{K}^{-1}$. This gives a value for g of $1.07 \times 10^{-7} \text{ s}^{-1}$, thus

$$\Delta\lambda \geq \sqrt{24 \times 60 \times 60 \times 1.07 \times 10^{-7}} = 0.096^{\text{rad}} = 5.5°$$

is always stable when using the stricter polar condition. The opposite end of the spectrum is the ocean-only system with no ice, where the heat capacity has value $C_{\text{ocean}} = 40 C_{\text{land}}$. This reduces the tolerance to $\Delta\lambda \geq 0.87°$.

Most models considered in this paper have a land-ocean fraction of $f_{\text{ocean}} = 0.7$ (i.e. 70% water). This corresponds to a value $\Delta\lambda = 0.018^{\text{rad}} = 1.03°$. The instability in the actual model can be found by varying the spatial dimension (thus $\Delta\lambda$), as seen in Fig. 1. The instability occurs around $\Delta\lambda \approx 1.23°$ which is reasonably close to the calculated value with the assumptions used.

3. EXOMOONS AND TIDAL HEATING

Habitable exomoons have a number of additional energy sources and sinks which can be added to the model to investigate their properties. We assume the exomoon is an Earth-like planet in orbit around a Jupiter-like gas giant.

The first energy source is emission from the body they are orbiting,

$$F_{\text{gas}} = \frac{\sigma T_{\text{gas}}^4}{4\pi a_{\text{moon}}^2}, \tag{18}$$

where T_{gas} is the temperature of the gas giant, and a_{moon} is the semimajoraxis of the moon around the giant. The temperature of the giant can be determined from eqn. (1). In the case of a giant such as Jupiter the temperature will actually be higher due to the excess heat of formation, though not by much [16].

The moon may also experience tidal heating, where due to the eccentricity of the orbit the forces on the moon produce stresses which heat the core and mantle of the planet. This heating can be quantified in two main methods.

The first and more simple method is Fixed-Q tidal heating. This is a constant heatflux through the surface of the moon and is given by,

$$F_{\text{fQ}} = \frac{21}{2} \frac{k}{Q} \frac{G^{3/2} M_{\text{gas}}^{5/2} R_{\text{moon}}^5 e_{\text{moon}}^2}{a_{\text{moon}}^{15/2}} \tag{19}$$

with k being the rigidity of the moon rock, Q is the quality coefficient. In this model the values of k and Q are fixed, hence fixed-Q model. A deficiency of this model is a prediction of tidal heat no matter how far away the moon is from the giant, and that the heatflux is constant no matter what happens to the moon.

The viscoelastic tidal heating model addresses these deficiencies by replacing the constant k/Q factor with the imaginary part of the second complex Love number, $\text{Im}(k_2)$:

$$F_{\text{tidal}} = \frac{21}{2} \text{Im}(k_2) \frac{G^{3/2} M_{\text{gas}}^{5/2} R_{\text{moon}}^5 e_{\text{moon}}^2}{a_{\text{moon}}^{15/2}}. \tag{20}$$

[14] [13] [15]. Finding the value of $\text{Im}(k_2)$ is difficult however as it is dependent on the $\text{Im}(k_2)$ function and the value of the temperature of the mantle of the planet.

The value of the tidal heating is calculated for a range of mantle temperatures and the convective cooling rate is also found for a range of mantle temperatures. The point at which these overlap is the mantle temperature where all the tidal heat flows through the surface of the planet. Finding the convective cooling rate involves an iterative process described in Henning et al 2009 [17].

Henning et al introduce four different viscoelastic response models: Maxwell, Voigt-Kelvin, SAS, Burgers. These models determine the $\text{Im}(k_2)$ function. Both the $\text{Im}(k_2)$ function and all associated functions are in appendix B. This paper focuses on the Maxwell model, due to the inherent simplicity. However, the code as written can be easily extended to work with the other more complicated models.

The third addition to the EBCM is a energy sink due to eclipsing of the moon by the giant. A 3 body gravity simulation can be used to find the average fraction of light eclipsed. Figure 2 shows how the amount of eclipsing varies with the semimajor axes and eccentricities of the moon and gas giant. The eclipsing is modelled as being 100% light blocked in the umbra, 50% light blocked in the penumbra, and 0% light blocked otherwise.

There is a linear relationship between Gas semimajor axis meaning there is more light eclipsed as the gas giant moves further from the star. This has a doubled effect as solar flux is decreasing by the square of the semimajor axis and an increasing amount of that light is being eclipsed.

Moon semimajor axis has the opposite relationship. As the moon's separation increases less light is blocked. This variablility is much more significant than the others, ranging from 15%
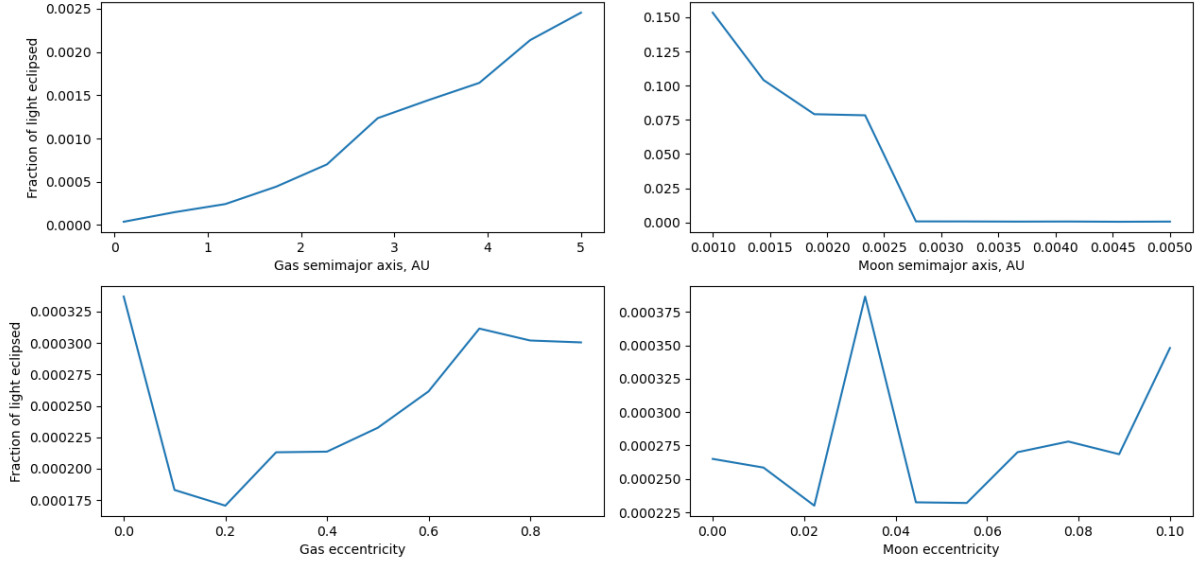
FIG. 2: Top Left: There is a positive correlation between the amount of light eclipsed and the distance of the gas giant from the star. Top Right: Negative correlation between the amount of light eclipsed and the distance of the moon to gas giant. Goes nearly to 0 but is still occasionally eclipsed but only the penumbra of the gas giant. Bottom Left and Bottom Right: Variations due to changing eccentricity, which are an order of magnitude smaller than the semimajor axis variations. This is due to averaging over many variable length eclipses to give a much smaller overall variation in eclipse length.

blocked down to nearly 0%. The largest drop is when the moon's orbit is far enough away that it is only ever in the penumbra of the gas giant.

In both cases varying eccentricity appears to have an effect which is an order of magnitude smaller than varying the semimajor axis. This is probably due to the averaging of many short and long eclipses to the same average eclipse time for 0 eccentricity.

Overall the effect of the eclipsing is minor except in instances where the orbit is extremely close to the gas giant, which would mostlikely result in large tidal heating which overpowers the small dip in flux.

4. CONVERGENCE TESTING OF 1D EBCM

Define a system to have converged if the global temperature average varies by less than a certain amount, ϵ_{tol}, between 2 averaging periods,

$$\frac{\Delta T}{T} = \frac{T_{\text{avg}}(t_2 \to t_3) - T_{\text{avg}}(t_1 \to t_2)}{T_{\text{avg}}(t_1 \to t_2)} \leq \epsilon_{\text{tol}}$$

where the global temperature is found from an area-weighted sum over all latitude bands in the time period,

$$T_{\text{avg}}(t_i \to t_j) = \frac{\sum_{n=i}^{j} \sum_{m=0}^{S-1} T_n^m \Delta t \cos(\lambda_m) \Delta \lambda}{\sum_{q=i}^{j} \Delta t \sum_{m=0}^{S-1} \cos(\lambda_m) \Delta \lambda}, \qquad (21)$$

the denominator evaluates to $2(t_j - t_i)$. The variables Δt and $\Delta \lambda$ can in general be variable for this expression, but in these simulations are constant.

Model Type	Semimajoraxis, au		Eccentricity		Obliquity	No. spatial nodes	Timestep	Land fraction type
	a_gas	a_moon	e_gas	e_moon	δ, deg	S	Δt, days	
Earth-like	1	-	0.0167	-	23.5	61	1	Uniform 70% Ocean
Tidal-heating	1	0.01	0.05	0.001	23.5	61	1	Uniform 70% Ocean

TABLE I: The default parameters for the models used in the analyses in the paper. A dashed entry, '-', indicates the value does not exist in the model. A 'Uniform' land fraction indicates that the model has the same ratio of land to ocean across the entire planet. An 'Earth-like' land fraction is not used, but is given in WK97 [6] and is an option in the code configuration file. The odd number of spatial nodes means there is a true equator with $\lambda = 0$ as well as poles with $\lambda = \pm 90°$
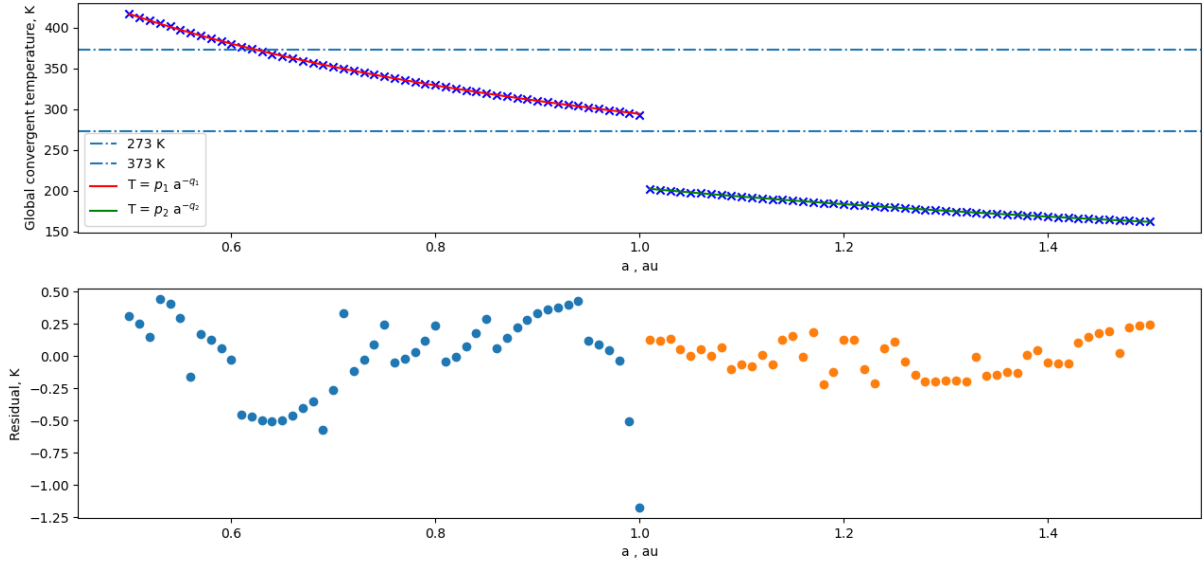

FIG. 3: Convergent global temperature of the Earthlike model varying semimajor axis and fitting to the theory prediction of $T \propto a^{-1/2}$ by the equation $T = p_i a^{-q_i}$. Also shown are 2 horizontal lines for the boiling and freezing points of water to roughly indicate habitability. There is a drop in the convergent temperature just after 1 au where the reduced insolation cannot prevent the planet from falling into a snowball state. The 'temperate' zone before 1 au fits with parameters $p_1 = 294.37 \pm 0.08$, $q_1 = 0.5026 \pm 0.0007$. The 'snowball' zone after 1 au instead fits parameters $p_2 = 203.5 \pm 0.6$, $q_2 = 0.5650 \pm 0.0009$. While the temperate zone follows the negative-half powerlaw very well, the snowball zone follows a slightly more negative powerlaw.

The orbital parameters of the model can then be varied to find habitable regions. The default parameters of the model are Earth-like, and are given in Table I.
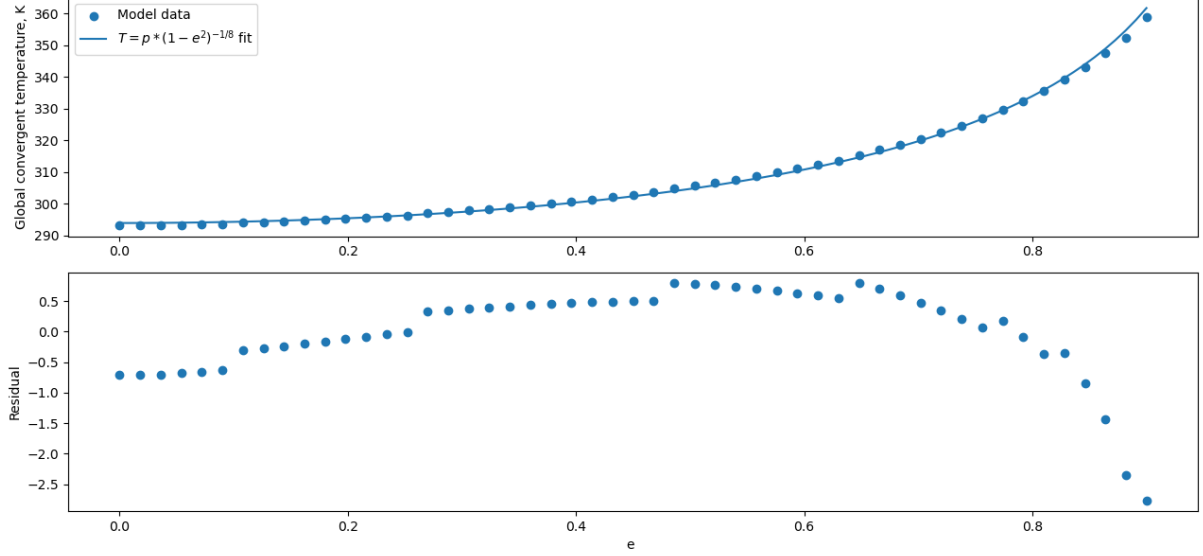
FIG. 4: Convergent Temperature of the Earthlike model varying eccentricity between 0 and 0.9. Overlaid on the data is a fit to the theory equation $T \propto (1 - e^2)^{-1/8}$, with proportionality constant $p = 293.89 \pm 0.10$ K. The fit is very good, with the extreme eccentricities diverging from the model slightly.

A. Investigating time-averaged solar flux

In their 2017 paper, Méndez and Rivera-Valentín show that for a planet in orbit with semi-majoraxis a and eccentricity e the average solar flux in an orbit is given by,

$$\langle F \rangle = \frac{L}{a^2 \sqrt{1 - e^2}}, \tag{22}$$

where L is the luminosity of the star, assumed to be constant (equation (14) in [8]). Subbing eqn. (22) into eqn. (1) the following temperature relation is found,

$$\frac{L}{a^2 \sqrt{1 - e^2}} (1 - A) = 4\sigma T^4, \tag{23}$$

where A is albedo and T is the temperature of the planet. Assuming that L and A are constant, we can see that T is proportional to $(1 - e^2)^{-1/8}$ for constant semimajoraxis and that T is proportional to $a^{-1/2}$ for constant eccentricity. These relations are confirmed by the model in Fig. 4 and Fig. 3 respectively.

We can also see that for a constant temperature $a \propto (1 - e^2)^{-1/4}$. This proportionality can be used to find how the inner (T = 273 K) and outer (T = 373 K) habitable zones scale with increasing eccentricity. It has been noted in Dressing10 that inner habitable zone follows this law quite closely but the outer zone has much greater variability due to other factors such as obliquity and ocean fraction. As shown in the left of Fig. 5, looking only at the temperature relation can lead to large deviations from the relation. However the scaling relation holds more closely by looking at the time and space averaged habitability on the right of the figure. This is due to the habitability calculation taking temperature extremes into account which the global average temperature would not.
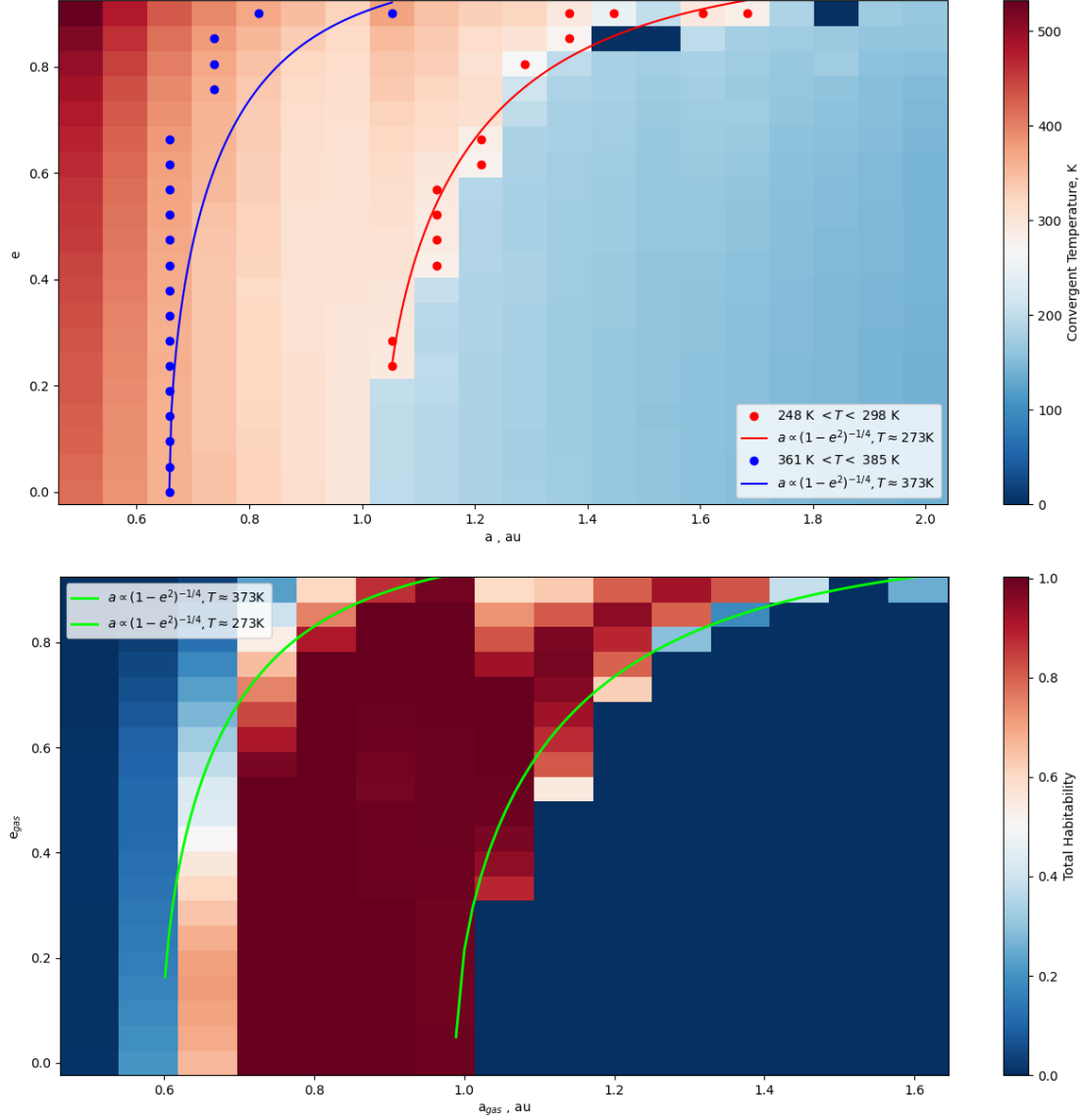
11

FIG. 5: Left: A heatmap of global average temperature, varying semimajoraxis and eccentricity of a uniform planet. Right: The same information but processed as global average habitability. Overlaid on both are the lines of constant temperature given by $a \propto (1 - e^2)^{-1/4}$ for $T = 273$ and $T = 373$ which represent the inner and outer habitable zones respectively. Since the temperature is never exactly 373 K or 273 K, a range of values are used to approximate the region. The three -1 K cells in the top left did not reach an equilibrium within 100 years of simulation. While the temperature line for 373 K is below the expected values, the corresponding line on the habitability graph follows the outer edge of the habitable region very well. This is indicative that global average temperature is not a good measure of habitability.

B.   Obliquity and Rotation speed

Understanding how the obliquity and rotation speed of the planet effects climate is also useful. Varying the obliquity can maximise or minimise the average temperature of the planet by changing how the energy is distributed over the planet's surface.
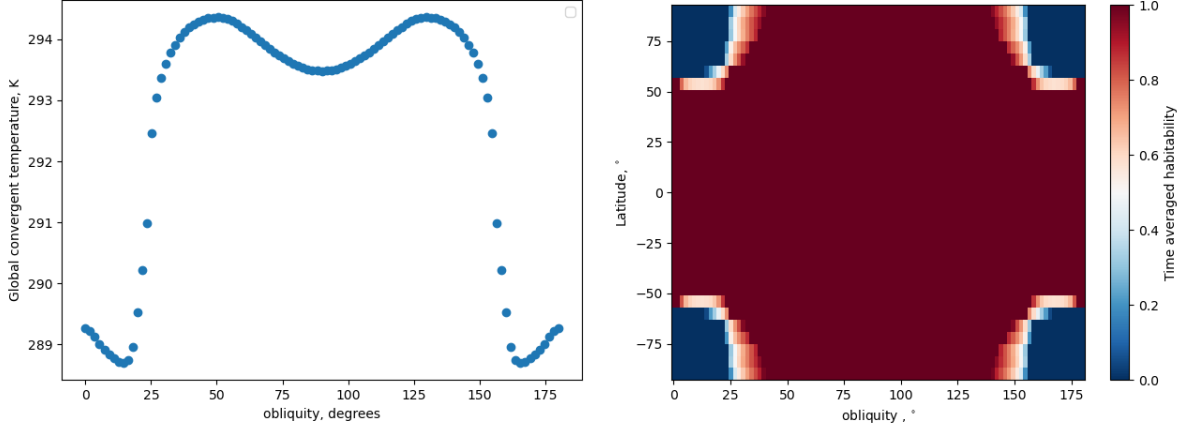
FIG. 6: Convergent Temperature of the Earthlike model varying obliquity between 0 and 180°. The data are symmetrical about 90°, as expected for a planet with a uniform surface. The plot indicates that there are optimal obliquities at $\delta \approx 20°$ and $\approx 50°$ for a minimum and maximum temperature respectively.

5.   1D ENERGY BALANCE DEPTH MODEL

So far the tidal heating has been found by balancing convection with tidal heat input, then allowing this tidal heat to flow through the surface of the planet. Now the tidal heat is allowed to flow through the bottom layer of a depth model. This investigates whether a planet with a cold frozen surface could harbour habitable temperatures below it's surface.

The depth model can be found by first considering the standard heat equation

$$\frac{\partial T}{\partial t} = \alpha \nabla^2 T, \tag{24}$$

and subbing the spherical form for the lapacian,

$$\frac{\partial T}{\partial t} = \alpha \left[\frac{1}{r} \frac{\partial^2}{\partial r^2}(rT) + \frac{1}{r^2 \sin\theta} \frac{\partial}{\partial \theta}\left(\sin\theta \frac{\partial T}{\partial \theta}\right) + \frac{1}{r^2 \sin\theta} \frac{\partial^2 T}{\partial \phi^2} \right] \tag{25}$$

where r is the distance to the center of the planet, $\theta = \pi - \lambda$ is the co-latitude θ related to the latitude λ, and ϕ is longitude. In the latitude-band surface case $T(r, \theta, \phi) = T(\theta)$ and the equation is transformed into λ, whereas in the depth case $T(r, \theta, \phi) = T(r)$.

Thus the depth model is given by

$$\frac{\partial T}{\partial t} = \alpha \left[\frac{\partial^2 T}{\partial r^2} + \frac{2}{r} \frac{\partial T}{\partial r} \right] \tag{26}$$

...

6.   CONCLUSIONS

Donec finibus, tellus sit amet luctus sodales, lectus ante accumsan ligula, at condimentum lorem justo a sapien. Phasellus vel tortor vitae metus lacinia efficitur ac vel ex. Aenean eget congue leo. Aliquam cursus mauris sit amet arcu dignissim, vel condimentum nisi sodales.

REFERENCES

[1] Courtney D. Dressing et al, HABITABLE CLIMATES: THE INFLUENCE OF ECCENTRICITY, ApJ, 721, 1295–1307, 2010

[2] Aomawa L. Shields et al, The Effect of Orbital Configuration on the Possible Climates and Habitability of Kepler-62f, Astrobiology, 16, 443-464, 2016

[3] Gerard Roe, In defence of Milankovitch, Geophysical Research Letters, 33, L24703, 2006

[4] David S. Spiegel et al, Habitable Climates, ApJ, 681, 1609–1623, 2008

[5] David S. Spiegel et al, Habitable Climates: the influence of Obliquity, ApJ 691, 596–, 2009

[6] Williams and Kasting, Habitable Planets with High Obliquities, Icarus, 129, 254-267, 1997

[7] North and Coakley, Differences between Seasonal and Mean Annual Energy Balance Model Calculations of Climate and Climate Sensitivity, J. Atmos. Sci., 36, 1189–1204, 1979

[8] Abel Méndez and Edgard G. Rivera-Valentín, The Equilibrium Temperature of Planets in Elliptical Orbits, ApJL, 837, 2017

[9] Viggo H. Hansteen, Numerical Modelling in a nutshell, University of Oslo, Institute of Theoretical Astrophysics, AST5110 Lecture materials 2011, accessed 6/11/2023: https://www.uio.no/studier/emner/matnat/astro/AST5110/h11/undervisningsmateriale/numerics_intro.pdf

[10] https://earthobservatory.nasa.gov/world-of-change/global-temperatures, paragraph 3, accessed 08/12/2023

[11] Sulaiman, Achilleos, Bertucci et al, Enceladus and Titan: emerging worlds of the Solar System, Exp Astron 54, 849–876, 2022

[12] Marc Rovira-Navarro et al, Tidally Heated Exomoons around Gas Giants, Planet. Sci. J., 2 119, 2021

[13] Segatz et al, Tidal dissipation, surface heat flow, and figure of viscoelastic models of Io, ICARUS 75, 187–206, 1988

[14] Charles F. Yoder, Stanton J. Peale, The tides of Io, Icarus, 47 1, 1–35, 1981

[15] Vera Dobos, René Heller, Edwin L. Turner, The effect of multiple heat sources on exomoon habitable zones, A&A 601 A91, 2017

[16] L. Li, X. Jiang, R.A. West et al, Less absorbed solar energy and more internal heat for Jupiter. Nat Commun 9, 3709, 2018

[17] Wade G. Henning et al, TIDALLY HEATED TERRESTRIAL EXOPLANETS: VISCOELASTIC RESPONSE MODELS, ApJ 707 1000, 2009

Appendix A: Numerical Stability Calculations

Take (6), set $S(1 - A) - I = 0$, and let $D/C = g$, thus:

$$\frac{\partial T}{\partial t} = g \left(\frac{\partial^2 T}{\partial \lambda^2} - \tan(\lambda) \frac{\partial T}{\partial \lambda} \right)$$

subbing in the discretisations, (7) (8) (9):

$$\frac{T_{n+1}^m - T_n^m}{\Delta t} = g \left(\frac{T_n^{m+2} - 2T_n^m + T_n^{m-2}}{(2\Delta\lambda)^2} - \tan(\lambda_m) \frac{T_n^{m+1} - T_n^{m-1}}{2\Delta\lambda} \right)$$

Then the planewave solution (12) can be plugged in and ξ solved for by dividing by (12):

$$\xi = 1 + g\Delta t \left(\frac{e^{2ik\Delta\lambda} - 2 + e^{-2ik\Delta\lambda}}{(2\Delta\lambda)^2} - \tan(\lambda_m) \frac{e^{ik\Delta\lambda} - e^{-ik\Delta\lambda}}{2\Delta\lambda} \right)$$

the first term in the brackets is equal to $-\sin^2(k\Delta\lambda)/\Delta\lambda^2$ and the second term is equal to $i \tan(\lambda_m) \sin(k\Delta\lambda)/\Delta\lambda$.

The absolute square can then be found as:

$$|\xi|^2 = 1 + \frac{g\Delta t \sin(k\Delta\lambda)^2}{\Delta\lambda^2} \left(g\Delta t \left(\tan(\lambda_m)^2 + \frac{\sin^2(k\Delta\lambda)}{\Delta\lambda^2} \right) - 2 \right)$$

subbing this into (13), the normal stability conditions are as follows:

$$g\Delta t \left(\tan(\lambda_m)^2 + \frac{\sin^2(k\Delta\lambda)}{\Delta\lambda^2} \right) \begin{cases} > 2 & \text{growing mode, unstable} \\ = 2 & \text{completely stable} \\ < 2 & \text{decaying mode, stable} \end{cases} \quad \text{(A1)}$$

The method to find the polar stability is much the same. subbing in discretisations (10) (or equally (11)) and (9), as well as the plane wave (12):

$$\frac{\xi^{n+1} - \xi^n}{\Delta t} = g \frac{\xi^n \exp(ik\Delta\lambda) - \xi^n}{(\Delta\lambda)^2}$$

where the exponential term in the plane wave is either 1 ($m = 0$) or $\exp(ik\Delta\lambda)$ ($m = 1$).

Dividing by ξ^n, and then solving for ξ:

$$\xi = 1 + \frac{g\Delta t}{(\Delta\lambda)^2} \left(\exp(ik\Delta\lambda) - 1 \right)$$

Leading to an absolute square magnitude given by

$$|\xi|^2 = 1 + 2(1 - \cos(k\Delta\lambda)) \frac{g\Delta t}{\Delta\lambda^2} \left(\frac{g\Delta t}{\Delta\lambda^2} - 1 \right)$$

And thus a polar stability condition of

$$(1 - \cos(k\Delta\lambda)) \frac{g\Delta t}{\Delta\lambda^2} \left(\frac{g\Delta t}{\Delta\lambda^2} - 1 \right) \begin{cases} > 0 & \text{growing mode, unstable} \\ = 0 & \text{completely stable} \\ < 0 & \text{decaying mode, stable} \end{cases} \quad .$$

The first term $\cos(k\Delta\lambda) - 1$ is equal to 0 when $k\Delta\lambda = 2\pi n$ for integer n. This implies that planewaves whose wavelengths are integer divisors of the node spacing are always stable at the poles.

Taking these solutions away, aswell as using that $\frac{g\Delta t}{\Delta\lambda^2} > 0$, the polar stability condition can be simplified to

$$\frac{g\Delta t}{\Delta\lambda^2} \begin{cases} > 1 & \text{growing mode, unstable} \\ = 1 & \text{completely stable} \\ < 1 & \text{decaying mode, stable} \end{cases} . \tag{A2}$$

Appendix B: Tidal heating and convective cooling

Maxwell model

$$\text{Im}(k_2) = \frac{57\eta\omega}{4\rho g R_{\text{moon}} \left[1 + \left(1 + \frac{19\mu}{2\rho g R_{\text{moon}}}\right)^2 \frac{\eta^2\omega^2}{\mu^2}\right]} \tag{B1}$$

functions for $\eta\mu$ are found in Henning09 [17].

convective heat flow to be equated to the maxwell model iteratively plug these equations into each other until there is very little change

$$q_{BL} = k_{\text{therm}} \frac{T_{\text{mantle}} - T_{\text{surf}}}{\delta(T)} \tag{B2}$$

$$\delta(T) = \frac{d}{2a_2} \left(\frac{Ra}{Ra_c}\right)^{-1/4} \tag{B3}$$

$$Ra = \frac{\alpha g \rho d^4 q_{BL}}{\eta(T)\kappa k_{\text{therm}}} \tag{B4}$$

$$\kappa = \frac{k_{\text{therm}}}{\rho C_p} \tag{B5}$$

SCIENTIFIC SUMMARY FOR A GENERAL AUDIENCE

Many interesting solar systems have been reported in the news, such as the Trappist-1 system which is filled with Earth-like planets. Simulations and models such as those in this paper are used to determine if a planet could be habitable. A habitable zone can be made by varying the parameters of the model to see where the model is habitable, partially habitable, or uninhabitable.

The main model in this paper takes a planet and divides it into a number of latitude bands which can have energy flow between them. Certain parameters, such as how the planet orbits around it's star and the angle the planet is tilted at, are varied to build this habitable zone. A result of this paper is if the Earth orbited slightly further away from the Sun then it is likely that it would fall into an ice age similar to what the Earth has experienced in the past. Another result found is that the tilt of the planet can affect how hot or cold it is, and indicates that the current tilt of the Earth gives a cold planet.

Another aspect of this paper's exoplanet research is exomoons orbiting a gas giant such as Jupiter. In certain configurations an exomoon can be heated not only from the host star, but also due to a process called tidal heating. Tidal heating is similar to stretching an elastic band. Stretching and relaxing an elastic band many times can cause the band to warm up. The moon of a gas planet is stretched slightly by unequal forces of gravity as one part of the moon is further away than the other. If the moon's orbit is not circular then the moon is stretched and relaxed, thus heats up in a similar way to the elastic band. Adding tidal heating to the model allows for investigations into how tidal heating can move, or change the shape of, the habitable zone.